


# Original Research

## Complement factor H deficiency combined with smoking promotes retinal degeneration in a novel mouse model

Liwen Feng<sup>1,2</sup> , Kailai Nie<sup>1,2</sup>, Qing Huang<sup>1</sup> and Wei Fan<sup>1</sup>

<sup>1</sup>Department of Ophthalmology, West China Hospital of Sichuan University, Chengdu 610041, China; <sup>2</sup>Research Laboratory of Ophthalmology and Vision Sciences, State Key Laboratory of Biotherapy, West China Hospital, Sichuan University, Chengdu 610041, China

Corresponding author: Wei Fan. Email: fanwei55@yahoo.com

### Impact statement

Age-related macular degeneration (AMD) is by far the leading cause of irreversible visual impairment in people over 60 years old, and there is no effective therapy for dry AMD. A mature animal model is of great significance for the study of this disease. Our study has generated a novel AMD murine model that combines known genetic and environmental risk factors to produce a relevant tool to analyze the pathophysiology and potential treatment of the disease in its early stages.

### Abstract

Age-related macular degeneration is the leading cause of blindness in the elderly. The Y402H polymorphism in complement factor H promotes disease-like pathogenesis, and a *Cfh*<sup>+/-</sup> murine model can replicate this phenotype, but only after two years. We reasoned that by combining CFH deficiency with cigarette smoke exposure, we might be able to accelerate disease progression to facilitate preclinical research in this disease. Wild-type and *Cfh*<sup>+/-</sup> mice were exposed to nose-only cigarette smoke for three months. Retinal tissue morphology and visual function were evaluated by optical coherence tomography, fundus photography and autofluorescence, and electroretinogram. Retinal pigment epithelial cell phenotype and ultrastructure were evaluated by immunofluorescence staining and

transmission electron microscopy. *Cfh*<sup>+/-</sup> smoking mice showed a dome-like protruding lesion at the ellipsoid zone (drusen-like deposition), many retinal hyper-autofluorescence spots, and a marked decrease in A- and B-wave amplitudes. Compared with non-smoking mice, wild-type and *Cfh*<sup>+/-</sup> smoking mice showed sub-retinal pigment epithelium complement protein 3 deposition, activation of microglia, metabolic waste accumulation, and impairment of tight junctions. Microglia cells migrated into the photoreceptor outer segment layer in *Cfh*<sup>+/-</sup> smoking mice showed increased activation. Our results suggest that exposing *Cfh*<sup>+/-</sup> mice to smoking leads to earlier onset of age-related macular degeneration than in other animal models, which may facilitate preclinical research into the pathophysiology and treatment of this disease.

**Keywords:** Complement factor H, smoking, AMD, animal model, macular degeneration

**Experimental Biology and Medicine 2021; 246: 1–10. DOI: 10.1177/15353702211052245**

### Introduction

Age-related macular degeneration (AMD) is by far the leading cause of irreversible visual impairment in people over 60 years old. In early stages of the disease, drusen and retinal pigment epithelium (RPE) dysfunction are observed, whereas the advanced stage involves either geographic atrophy or neovascularization. Most patients (80%) have non-exudative or dry AMD, for which there is no effective therapy.<sup>1</sup> The pathogenesis of AMD is complex, and it involves genetic polymorphisms and environmental factors. Currently, more than 50 susceptibility genes have been identified, among which *CFH* and *ARMS2* genes are

the most important in pathogenesis.<sup>2</sup> Environmental risk factors include smoking, unhealthy diet, obesity, high blood pressure, hypercholesterolemia, and antioxidant deficiency. The Y402H polymorphism is the single nucleotide polymorphism of *CFH*. This mutation may impair the binding efficiency and other molecule function, and hence reduce the inhibitory abilities of CFH, resulting in the over-activation of complement alternative pathway at the interface between RPE and Bruch's membrane. Epidemiological studies suggest that carriers of the *CFH* Y402H mutation and heavy smokers are at higher risk of AMD.<sup>3</sup> Multiple studies have confirmed the association

between Y402H polymorphism in *CFH* and increased risk of AMD.<sup>4,5</sup>

Although mice do not have a macula, their retinal structures are similar to those of the peripheral retinas in humans, and they can exhibit the characteristics of dry AMD.<sup>6</sup> Deleting or decreasing expression of the *Cfh* gene predisposes mice to AMD.<sup>7-10</sup> *Cfh*<sup>-/-</sup> mice show significantly greater stress responses and inflammation in an open environment than in a pathogen-free environment.<sup>11</sup> These findings suggest that when *CFH* is deficient, environmental risk factors may contribute to a more severe phenotype.

Cigarette smoke, which increases the risk of AMD by two to four folds,<sup>12</sup> is the leading preventable risk factor, and it synergizes with mutations in certain genes to further increase risk of the disease.<sup>13</sup> Several groups have described a mouse model in which AMD can be initiated through cigarette smoke exposure,<sup>14-16</sup> an effect that involves activation of the complement system.<sup>17</sup> Indeed, complement inhibitors can prevent and even repair smoking-induced ocular injury.<sup>18</sup> These findings suggest that there is a close association between cigarette smoke exposure and complement activation.

Studies with the previously described mouse models of AMD can take a long time, since two years may be needed for the disease phenotype to manifest.<sup>8</sup> We reasoned that combining excessive complement activation with cigarette smoke exposure might accelerate development of the disease in mice. If so, the resulting animal model could support more efficient and extensive preclinical studies into disease onset, progression, and treatment.

## Materials and methods

### Generation of *Cfh*<sup>+/-</sup> mouse

The CRISPR/Cas-9 system was used to generate homozygous *Cfh* knockout (*Cfh*<sup>-/-</sup>) mice. Two single-guide RNAs were designed to target exons 2 and 3 in the mouse *Cfh* gene (ENSMUSG00000026365):<sup>19</sup> sgRNA1, CCGTATATGAACG GATGATCAGG; and sgRNA2, TCATCCTACGTAGGAT TAGCAGG. The sgRNAs were synthesized and inserted into the Cas9 vector plasmid (pRP [CRISPR]-Hcas9-U6, VectorBuilder, China), then transformed into *E. coli* and amplified. The amplicons were purified for DNA sequencing. The linearized DNA was transcribed and amplified into RNA, and the purified RNA was identified by electrophoresis. The diluted RNA was microinjected into mouse fertilized eggs, and then the eggs were transferred into pseudopregnant female C57BL/6 mice. After giving birth to mice, F1 generation mice were obtained. Tail tissue was harvested for Sanger sequencing and PCR genotyping. The primers used were F, ATGTGTTTAAGCCCAAATCTG CTCC; *Cfh*-R, GAGGCAACAATGAGTTCAAGAAACCA; and He/Wt-R, AACTTCTTCTCTCCCTCGCCCAT. All wild-type (WT) C57BL/6 mice were purchased from Beijing HFK BioScience (Beijing, China).

Mice were housed on a 12-h light/dark cycle and received food and water ad libitum. All procedures were conducted in compliance with the Association for Research

in Vision and Ophthalmology (ARVO) statement and approved by the Animal Ethics Committee of West China Hospital of Sichuan University (approval number: 2019280 A).

### Grouping of animals and treatments

Since the complement system of *Cfh*<sup>-/-</sup> mice may be deficient,<sup>9</sup> the mice can develop severe membranoproliferative glomerulonephritis, leading to death at 12 to 24 months.<sup>19</sup> Therefore, *Cfh*<sup>+/-</sup> mice were selected for this study. Estrogen level affects the formation of subretinal deposits,<sup>20</sup> so all mice in this study were male. Eight-week-old male mice were randomly divided into smoking or non-smoking groups for a total of four conditions: WT non-smoking ( $n=10$ ), WT smoking ( $n=20$ ), *Cfh*<sup>+/-</sup> non-smoking ( $n=10$ ), and *Cfh*<sup>+/-</sup> smoking ( $n=20$ ). Smoking groups were exposed to smoke using a nose-only cigarette smoke exposure method as described.<sup>21</sup> Briefly, the mouse was restrained in a custom-designed container, and the container was mounted in a smoking chamber in which the cigarette smoke flowed in one direction. There were closed-pipe connections linking the smoking chamber, the fixed-rate pump (CH Technologies, Westwood, NJ, USA), and the Baumgartner-Jaeger CSM2082i automated cigarette smoke machine (CH Technologies, West-Wood, NJ, USA). Commercially available cigarettes (Marlboro, Philip Morris, USA) were used to generate smoke. The cigarette smoke was diluted with fresh air (2.6:9.1) to obtain a concentration of total suspended particulates of 250 mg/m<sup>3</sup>. The mice were exposed to cigarette smoke two times/day for 75 min/time during 12 weeks. Non-smoking mice were maintained under standard husbandry conditions for 12 weeks.

### OCT, fundus photography, FAF examination, and ERG

Mice were sedated with an intraperitoneal injection of chloral hydrate (4  $\mu$ l/g). Then, tropicamide eye drops (Santen Pharmaceutical, Japan) and oxybuprocaine hydrochloride eye drops (Santen Pharmaceutical) were administered to provide pupil dilatation and topical anesthesia, respectively. OCT, fundus photography, and FAF examinations were performed using the Spectralis imaging platform (Spectralis HRA + OCT, Heidelberg, Germany). Images were analyzed for fluorescing spots using ImageJ (<http://imagej.net/ImageJ>, version 1.52a, USA); the number of fluorescing spots of one retina was manually counted. Retinal function was evaluated using flash ERG (RetiMINER IV, IRC, China). Mice were dark-adapted overnight before anesthesia and pupil dilatation, and experiments were performed under dim red illumination.

### Immunofluorescence staining

Mice were sacrificed by cervical dislocation under general anesthesia. Eyes were enucleated immediately, then a hole was punched at the limbus, and the punch biopsy was fixed in 4% paraformaldehyde for 40 min at room temperature. After dehydration and embedding at optimal cooling temperature, cryo-sections were made at a thickness of 6  $\mu$ m.

Immunofluorescence staining was performed for C3b/iC3b/C3c, IBA1, rhodopsin, and IB4. The sources and dilutions of all antibodies are listed in Table S1. Images were captured using the Axio Imager Z2 fluorescence microscope (Zeiss, Germany). RPE-choroid-sclera flat-mounts were prepared<sup>22</sup> for ZO-1 immunofluorescence staining, and an A1RMP+ confocal microscope (Nikon, Japan) was used to capture images. For quantitative analysis, the number of activated microglia cells was manually counted using ImageJ software.

### Transmission electron microscopy

Mice were sacrificed, eyes were enucleated, and a hole was punched at the limbus using a 29G needle. Eyeballs were fixed in electron microscopy fixative (Servicebio, China) at 4°C. The fixed tissues were cut into 1-mm<sup>3</sup> cubes on clean filter paper. After osmium fixation, acetone gradient dehydration, embedding agent infiltration, and polymerization, the tissue pieces were cut into 70-nm sections, which were then double-stained with uranium acetate and citric acid. Images were obtained using an H7650 TEM (Hitachi, Japan).

### Statistical methods

Numerical data were processed using Microsoft Excel (version 2013), and graphs were generated using GraphPad Prism 6.0 for Windows (GraphPad Software, Bethesda, MD, USA). Appropriate statistical methods were selected according to the type of data. For the comparison of the number of fluorescing spots between *Cfh*<sup>+/-</sup> smoking and *Cfh*<sup>+/-</sup> non-smoking mice, an independent-samples t-test with unequal variances was chosen. ANOVA with post hoc Dunnett T3 or Tukey HSD test was chosen to assess differences in the numbers of activated microglia cells and the ERG amplitudes among the four groups. Statistical analyses were performed using SPSS 13.0 for Windows (SPSS, Chicago, IL, USA), and differences associated with  $P < 0.05$  were considered significant.

## Results

### Genotyping of *Cfh* knockout mice

*Cfh* knockout was confirmed by Sanger sequencing in mice of the first filial (F1) generation, and we determined the genotype of the resulting offspring by polymerase chain reaction (PCR) and agarose gel electrophoresis (Figure 1). The results indicated that the CRISPR-Cas9 system was effective in knocking out the *Cfh* gene. *Cfh*<sup>+/-</sup> mice were used in all of the following experiments.

### Smoking and CFH deficiency impaired visual function

Photoreceptor degeneration and retinal function were assessed using electroretinography (ERG), which is a useful tool in the early diagnosis of AMD.<sup>23,24</sup> Decreased A- and B-wave amplitudes are one of the hallmarks of early AMD.<sup>25</sup> The ERG responses of all mouse groups under scotopic conditions are presented in Figure 2(a). The data showed that the amplitudes of A- and B-waves gradually

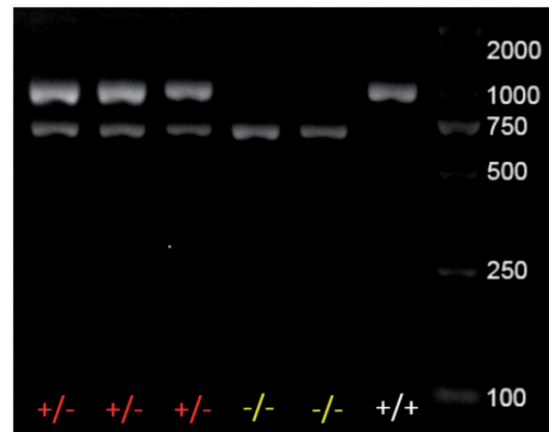


**Figure 1.** Genotyping of mice. Polymerase chain reaction (PCR) and agarose gel electrophoresis to genotype the progeny. (A color version of this figure is available in the online journal.)

increased with increasing stimulus intensity in all groups. Differences in B-wave amplitudes among all groups were significant at stimulation intensities of 0.01 ( $P = 0.005$ ), 0.1 ( $P = 0.011$ ), 1.0 ( $P < 0.001$ ), and 3.0 ( $P = 0.014$ ); differences in A-wave amplitudes were significant at intensities of 0.1 ( $P = 0.028$ ), 1.0 ( $P = 0.001$ ), and 3.0 ( $P = 0.002$ ) (Figure 2 (b)). A- and B-wave amplitudes of ERG responses in the *Cfh*<sup>+/-</sup> smoking group were markedly decreased at some stimulus intensities.

Differences between *Cfh*<sup>+/-</sup> smoking and *Cfh*<sup>+/-</sup> non-smoking mice in A-wave amplitudes were significant at stimulation intensities of 1.0 (ANOVA, post hoc Tukey HSD,  $P = 0.001$ ) and 3.0 (ANOVA, post hoc Tukey HSD,  $P = 0.006$ ), while differences in B-wave amplitudes were significant at an intensity of 1.0 (ANOVA, post hoc Dunnett T3,  $P = 0.002$ ) (Figure 2(b)).

Compared with WT non-smoking mice, WT smoking mice showed significantly decreased A-wave amplitudes only at a stimulation intensity of 3.0 (ANOVA, post hoc Tukey HSD,  $P = 0.045$ ). Compared with WT smoking mice, *Cfh*<sup>+/-</sup> smoking mice showed lower A-wave amplitudes at stimulation intensities of 0.1 (ANOVA, post hoc Dunnett T3,  $P = 0.017$ ) and 1.0 (ANOVA, post hoc Tukey HSD,  $P = 0.017$ ) (Figure 2(b)). Since A-wave amplitude reflects rod photoreceptor function,<sup>26</sup> our data indicate that rod photoreceptor function is compromised in WT smoking mice and to an even greater extent in *Cfh*<sup>+/-</sup> smoking mice. This was further confirmed by anti-rhodopsin immunofluorescence staining which also showed the structure of photoreceptors were injured in *Cfh*<sup>+/-</sup> smoking mice (Figure 3).

### Smoking and CFH deficiency impaired retinal pigment epithelial cells

While fundus imaging revealed no drusen or other AMD-like pathology in *Cfh*<sup>+/-</sup> smoking or non-smoking mice after 12 weeks (Figure 4(a)), fundus autofluorescence (FAF) showed a large number of hyper-autofluorescence spots in a speckled pattern in *Cfh*<sup>+/-</sup> smoking mice (Figure 4(b)). FAF in the *Cfh*<sup>+/-</sup> non-smoking mice revealed

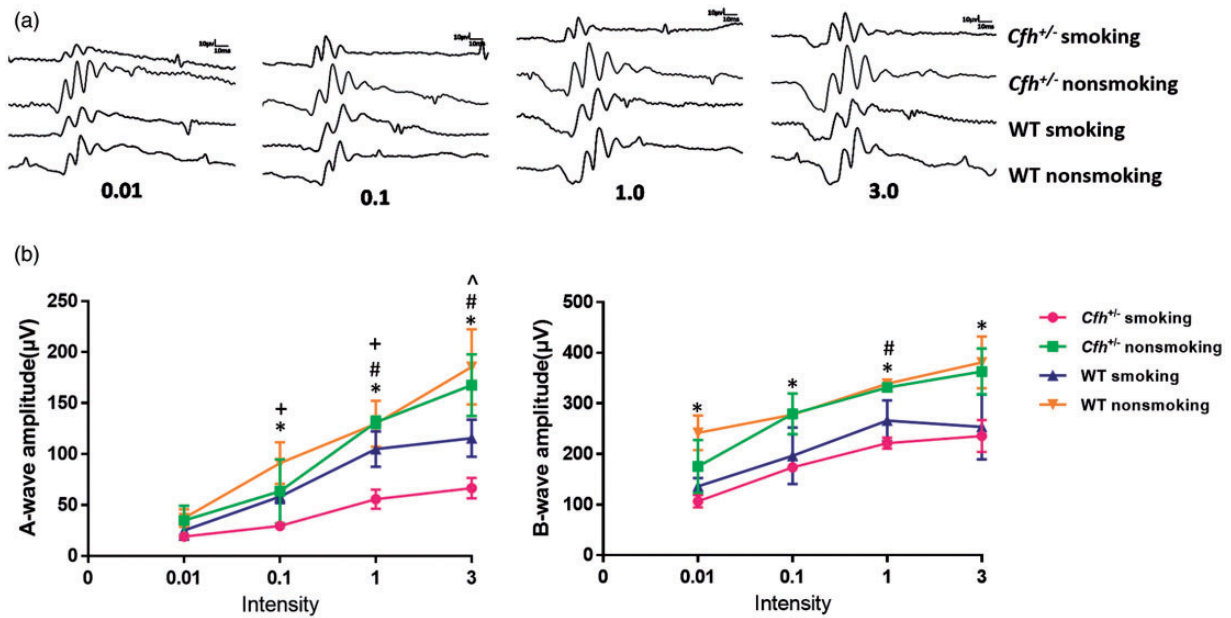


**Figure 2.** Electroretinograms of visual function in mice. (a) Amplitudes increased with flash stimuli of increasing intensity. (b) Differences in A- and B-wave amplitudes among all groups (ANOVA) (\*) ( $n = 3$ ). *Cfh*<sup>+/-</sup> smoking mice showed significantly lower A- and B-wave amplitudes than *Cfh*<sup>+/-</sup> non-smoking mice (#) and WT smoking mice (+). “^” means the amplitudes of WT smoking mice was significantly lower than WT non-smoking mice. (A color version of this figure is available in the online journal.)  
WT: wild-type.

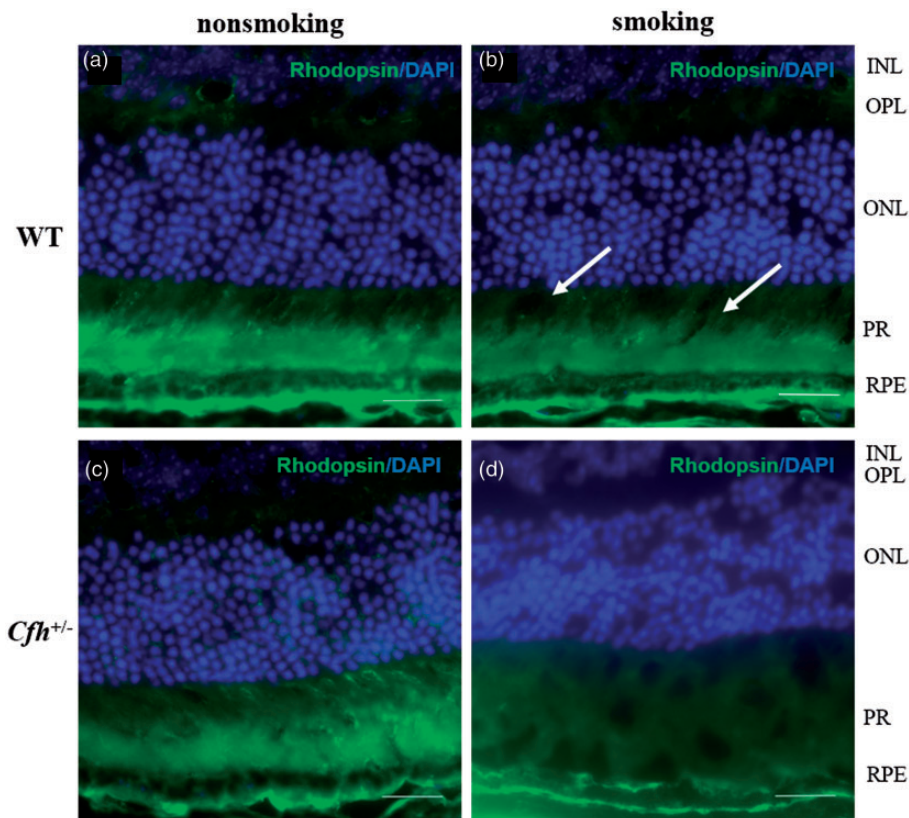


**Figure 3.** Immunofluorescence of rhodopsin. Rhodopsin staining showed the morphology and structure of photoreceptors. (a and c) *Cfh*<sup>+/-</sup> and WT non-smoking mice showed the intact photoreceptor structure; (b) in WT smoking mice, most of the relatively intact photoreceptor structure was preserved, with only a small amount of lesions (arrows). (d) Photoreceptor cells were not intensely labeled. Marked swelling and structural disorder in the photoreceptor of the *Cfh*<sup>+/-</sup> smoking mice. Scale: 20 µm. (A color version of this figure is available in the online journal.)  
WT: wild-type; INL: inner nuclear layer; OPL: outer plexiform layer; ONL: outer nuclear layer; RPE: retinal pigment epithelium; PR: photoreceptor.

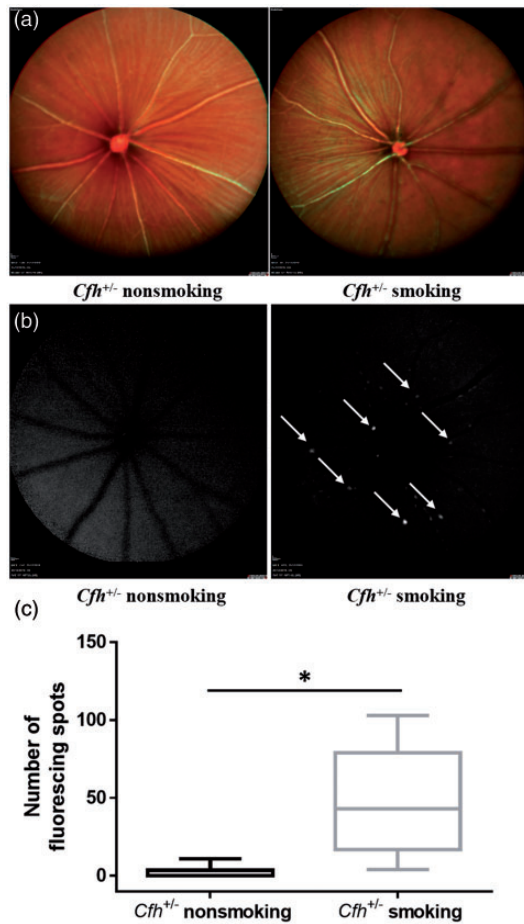


**Figure 4.** RPE cell dysfunction caused by smoking and CFH deficiency. (a) Fundus photography showed normal appearance of the fundus in *Cfh*<sup>+/+</sup> smoking and non-smoking mice. (b) Fundus autofluorescence (FAF) showed a large number of hyper-autofluorescence spots (arrows) in a speckled pattern in the *Cfh*<sup>+/+</sup> smoking mice. (c) The box plots represent the number of hyper-autofluorescence spots in the *Cfh*<sup>+/+</sup> smoking mice ( $n = 3$  mice, six eyes) and *Cfh*<sup>+/+</sup> non-smoking mice ( $n = 4$  mice, eight eyes). The number of hyper-autofluorescence spots was significantly greater in the *Cfh*<sup>+/+</sup> smoking mice ( $t = 3.094$ ,  $P = 0.026$ ). (A color version of this figure is available in the online journal.)

normal fundus appearance (Figure 4(b)). These FAF findings indicate that RPE cells of *Cfh*<sup>+/+</sup> smoking mice contained significantly more lipofuscin and other metabolic waste products than RPE cells of *Cfh*<sup>+/+</sup> non-smoking mice.

Anti-ZO-1 immunofluorescence staining of RPE-choroidal-sclera flat-mounts revealed a blurred and interrupted RPE cell tight junction in WT and *Cfh*<sup>+/+</sup> smoking mice (Figure 5(c) and (d)), suggesting that there was significant damage to tight junctions of RPE cells. The destruction of tight junctions was more extensive in *Cfh*<sup>+/+</sup> smoking mice than in WT smoking mice (Figure 5(c)). In the *Cfh*<sup>+/+</sup> and WT non-smoking mice, the tight junctions were intact and clearly visible between adjoining cells (Figure 5(a) and (b)).

Transmission electron microscopy (TEM) demonstrated an accumulation of intracellular granules in RPE cells of *Cfh*<sup>+/+</sup> smoking mice, which might be undigested shed photoreceptor outer segments, lipofuscin particles, or

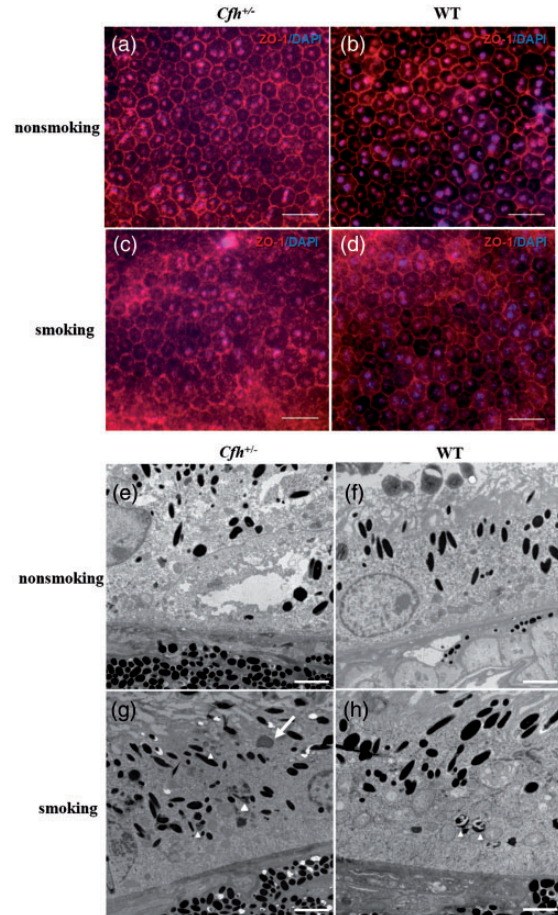


**Figure 5.** Retinal pigment epithelial (RPE) cell morphology. (a–d) Anti-ZO-1 immunofluorescent staining of RPE-choroidal-sclera flat-mounts. (c) The RPE cell tight junctions of *Cfh*<sup>+/+</sup> smoking mice were blurred, interrupted, and more severely damaged than those in WT smoking mice (d). (a and b) The RPE cell tight junctions in non-smoking mice were intact and clear. ZO-1 staining appears red and nuclear staining with DAPI appears blue. Scale: 20  $\mu$ m. (g) The ultra-structure of RPE cells in *Cfh*<sup>+/+</sup> smoking mice, as revealed by transmission electron microscopy, showed undigested shed photoreceptor extracellular segments (long arrow), lipofuscin, and other particles (triangle). (h) Melanin was disintegrated in RPE cells of WT smoking mice (triangle). Scale: 2  $\mu$ m. (A color version of this figure is available in the online journal.)

other substances. Basement folds and Bruch's membranes were generally normal (Figure 5(g)). These results indicate that smoking and CFH deficiency can lead to phagocytic and digestive dysfunction as well as structural impairment in murine RPE cells.

### Smoking and CFH deficiency resulted in complement system activation and deposition of complement activation products

Optical coherence tomography (OCT) showed drusen-like accumulation at the posterior pole of the eye in *Cfh*<sup>+/+</sup> smoking mice, with a dome-shaped protrusion extending into the ellipsoid zone (Figure 6(a)). In contrast, *Cfh*<sup>+/+</sup> non-smoking mice were phenotypically normal. Immunofluorescence staining for C3b/iC3b/C3c showed normal histological findings in non-smoking WT and *Cfh*<sup>+/+</sup> mice (Figure 6(b) and (d)), but subretinal deposits of complement activation products in *Cfh*<sup>+/+</sup> and WT

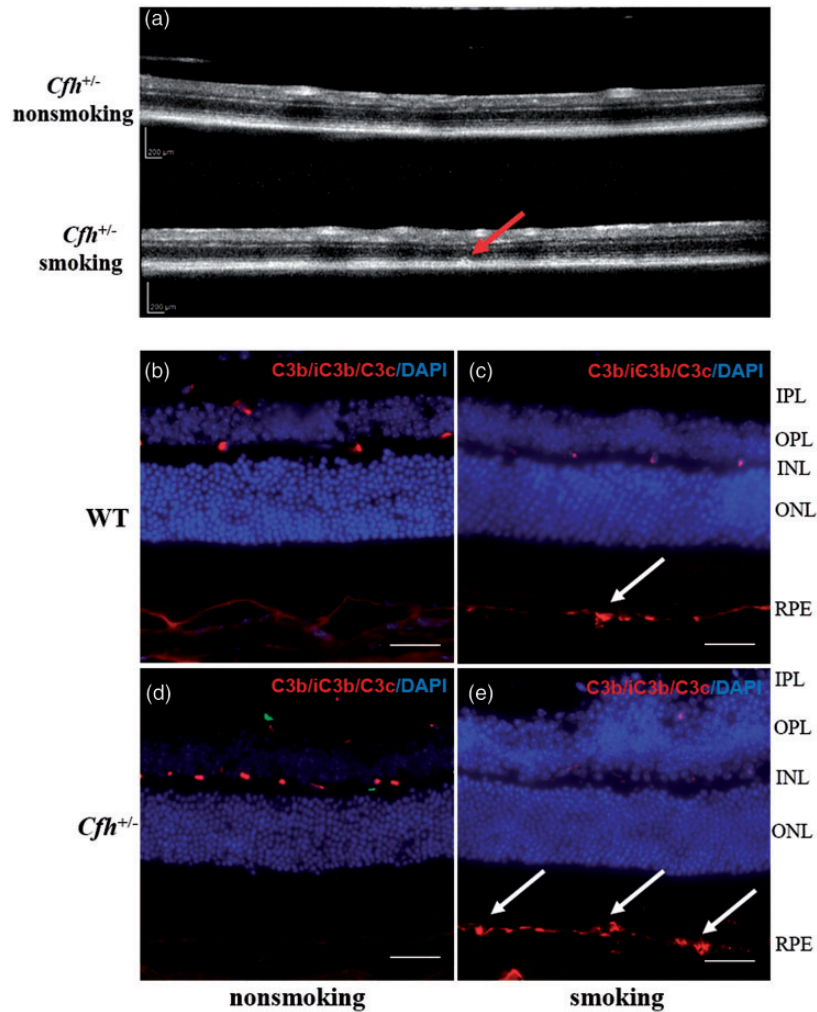


**Figure 6.** Complement system activation and deposition of complement activation products. (a) Optical coherence tomography (OCT) showed a Drusen-like accumulation in *Cfh*<sup>+/-</sup> smoking mice and normal morphology in non-smoking mice. (c and e) C3b/iC3b/C3c immunofluorescence staining revealed deposition of complement products in the sub-RPE of smoking mice, while C3b/iC3b/C3c were occasionally scattered in the OPL, IPL, and GCL (where the retinal vessels are located) in non-smoking animals (b and d). C3b/iC3b/C3c staining appears red, while nuclear staining by DAPI appears blue. Scale: 50 μm. (A color version of this figure is available in the online journal.)

GCL: ganglion cell layer; IPL: inner plexiform layer; INL: inner nuclear layer; OPL: outer plexiform layer; ONL: outer nuclear layer; RPE: retinal pigment epithelium.

smoking mice (Figure 6(c) and (e)). These results suggest that smoking and CFH deficiency could hyperactivate the retinal complement system and cause deposition of complement activation products.

### Smoking and CFH deficiency caused retinal microglial activation

Iba1 immunofluorescence showed slight activation of microglial cells in the WT smoking mice, indicated by the dendrites of microglia extending into the outer nuclear layer. In *Cfh*<sup>+/-</sup> smoking mice, we detected the migration of microglia into the outer segment layer of photoreceptor cells, which is characteristic of AMD (Figure 7(d)). No microglial activation was observed in the non-smoking group (Figure 7(a) and (c)). The difference in microglial activation among the four groups was statistically significant ( $P < 0.001$ ), and the post hoc Dunnett T3 test indicated that the number of activated microglial cells was significantly higher in *Cfh*<sup>+/-</sup> smoking mice than in *Cfh*<sup>+/-</sup>

non-smoking ( $P = 0.001$ ), WT smoking ( $P = 0.003$ ), and WT non-smoking ( $P = 0.001$ ) mice (Figure 7(e)). The difference in the number of activated microglial cells between WT smoking and WT non-smoking mice was statistically significant based on the independent-samples t-test ( $P = 0.028$ ) (Figure 7(e)).

Retinal tissue sections from *Cfh*<sup>+/-</sup> smoking mice were also stained with anti-Iba1 and -IB4 antibodies to evaluate neovascularization and its spatial relationship to these activated microglial cells. There was no co-localization of the stains, suggesting that there was no neovascularization at the sites to which microglia had migrated. In fact, no neovascularization was found anywhere in the retina of *Cfh*<sup>+/-</sup> smoking mice (Figure 7(f) to (i)). These findings suggest that smoking can induce the activation of microglia and retinal inflammation, and that in a smoking background, abnormal activation of the complement system (i.e. in *Cfh*<sup>+/-</sup> mice) further activates microglia and exacerbates inflammation.

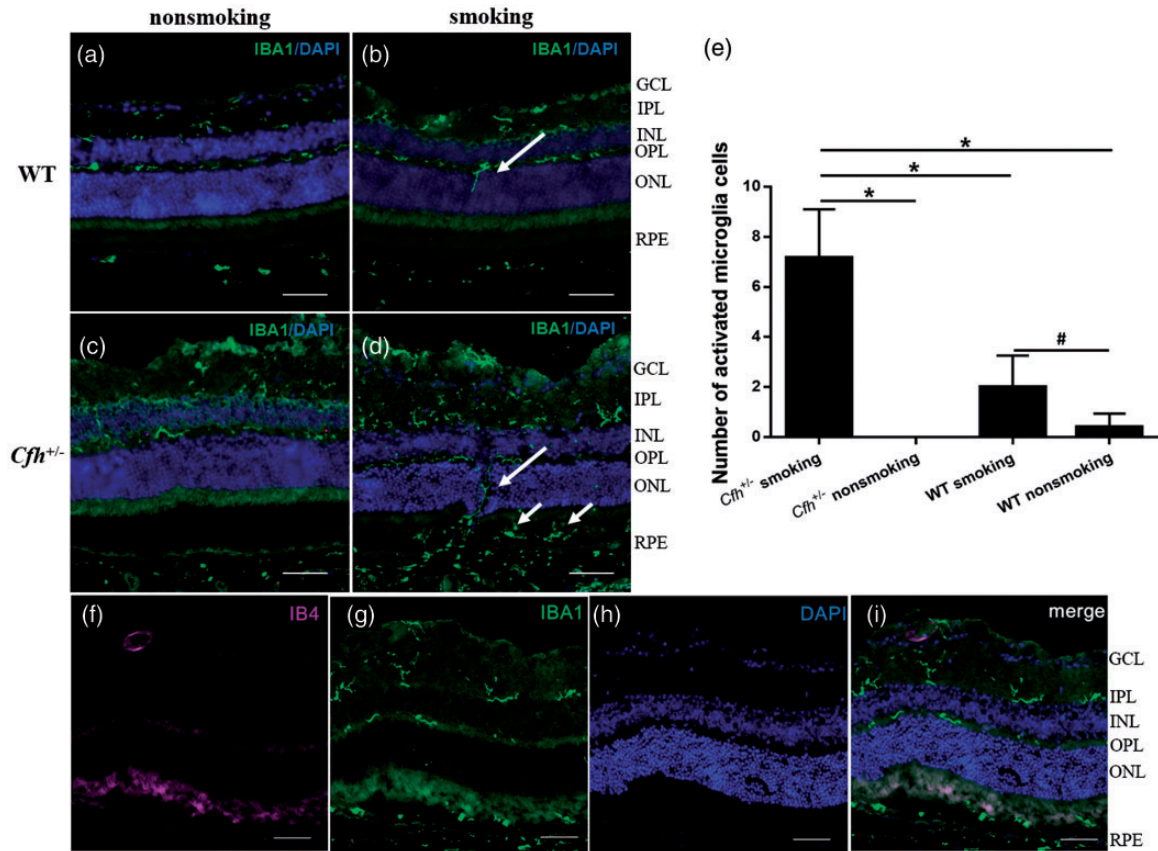


**Figure 7.** Microglial cell activation. (a and c) WT and *Cfh*<sup>+/-</sup> non-smoking mice showed quiescent microglia located in OPL, INL, and GCL regions. (b and d) In the WT and *Cfh*<sup>+/-</sup> smoking mice, the dendrites of microglia extended into the outer nuclear layer (long arrows); (d) in the *Cfh*<sup>+/-</sup> smoking mice, microglia migrated into the outer segment layer of photoreceptor cells (short arrows) Scale: 50  $\mu$ m. (f–i) Co-staining against Iba1 and IB4 showed there was no neovascularization in the *Cfh*<sup>+/-</sup> smoking mice. Scale: 50  $\mu$ m. (e) Quantification of activated microglial cells per field of view. *Cfh*<sup>+/-</sup> smoking mice showed greater microglial activation than any other group. Data are presented as mean  $\pm$  SD ( $n = 5$ –6 per group). \* $P < 0.01$  by ANOVA; # $P < 0.05$  by t-test. (A color version of this figure is available in the online journal.) GCL: ganglion cell layer; IPL: inner plexiform layer; INL: inner nuclear layer; OPL: outer plexiform layer; ONL: outer nuclear layer; RPE: retinal pigment epithelium.

## Discussion

This study provides a new animal model of AMD that may facilitate more extensive and faster preclinical studies to understand the pathology and treatment of the disease. We found that the combination of complement system over-activation and cigarette smoke exposure accelerated and strengthened the AMD-like phenotype of *Cfh*<sup>+/-</sup> mice, leading them to present features characteristic of early-onset AMD, including RPE cell dysfunction, deposition of complement activation products, activation of microglia, and impairment of visual function.

### The complement system and AMD

The retina is an immune-privileged tissue whose blood-retina barrier protects it from damage caused by pathogenic factors. In addition to immune avoidance and tolerance, innate defense systems, including microglia and the complement system, also protect the retina. The normal function of the complement system is essential for the maintenance of the normal retinal immune microenvironment,<sup>27,28</sup> and it plays a key role in host-defense against pathogens. However, it must be strictly regulated to avoid inflammation and tissue damage. There are three complement activation pathways: the typical, lectin, and

alternative pathways. The alternative pathway is initiated by the spontaneous hydrolysis of protein C3. Activation of the alternative pathway is spontaneous and continuous. AMD involves hyperactivation of the alternative complement pathway. As a crucial inhibitor of the alternative complement pathway, CFH affects the progression of AMD by regulating oxidative stress, inflammation, and abnormal angiogenesis.<sup>29</sup> Moreover, the antioxidant stress function of CFH is independent of its ability to inhibit the formation of the membrane attack complex.<sup>30</sup>

Our results showed that *Cfh*<sup>+/-</sup> non-smoking mice had normal retinal morphology over 20 weeks, without an AMD-like phenotype. The AMD phenotype requires a long period to develop if only driven by an abnormally activated complement system.<sup>10</sup> This suggests that CFH deficiency might contribute to AMD initiation and progression, but low expression of CFH alone is not sufficient to induce retinal degeneration in young mice. Alternatively, there may be some mechanisms to compensate for the CFH deficiency.

### Smoking, complement activation, and AMD

A large number of studies showed that cigarette smoke could induce RPE cell apoptosis, basal laminar deposits,

thickened Bruch's membrane, impaired visual function, and other AMD-like changes in mice.<sup>14,15,31,32</sup> In our study, we confirmed some of those changes in the WT smoking mice. The visual function of WT smoking mice was impaired, as shown by the decreased A-wave amplitudes in ERG. Under normal conditions, the RPE is one of the tissues with the highest oxygen consumption, and it is sensitive to anoxia and oxidants. Oxidants in cigarette smoke appear to underlie the pathology that harms RPE cells,<sup>33</sup> which is closely related to the early development of AMD.<sup>34</sup> It is well known that the RPE cells are part of the outer blood-retina barrier, and dysregulation of RPE integrity involves retinopathies, including AMD<sup>35</sup>. We found that the tight junctions between RPE cells in the WT smoking mice were destroyed, demonstrating that smoking disrupts this critical blood-retina barrier. Furthermore, we showed that the complement-activation product C3b/iC3b/C3c is deposited in the sub-RPE in WT smoking mice, which is consistent with results from other studies.<sup>36,37</sup> This provides direct evidence that smoking can lead to complement system activation. Finally, we found that microglia in the retina were slightly activated in WT smoking mice, and that the number of activated microglia cells was significantly higher, suggesting that smoking alone can activate immune cells in mice with otherwise normal immune function. With age and in the presence of risk factors such as smoking, RPE cells change from an inflammatory state that attempts to restore homeostasis to a state of chronic inflammation associated with AMD.<sup>38</sup> The change in the immune microenvironment of retinas in smoking mice may initiate AMD.

Studies have shown that *Cfh*<sup>+/-</sup> mice at 90 weeks displayed AMD-like characteristics, while the mice under 40 weeks showed no similar changes.<sup>10</sup> *Cfh*<sup>-/-</sup> mice fed under normal feeding conditions for 96 weeks also showed AMD-like changes,<sup>9</sup> indicating that age plays an important role in the pathogenesis of AMD. However, *Cfh*<sup>-/-</sup> mice fed with low glycemic index chow showed early AMD-like characteristics at the age of 10 months (40 weeks),<sup>39</sup> which was more than twice as quickly as mice fed a normal diet. The authors speculated that this might be because the low-energy diet leads to oxidative stress and dysfunction of RPE cells. Under CFH deficiency, the ability of the retina to inhibit oxidative stress could then be considerably weakened, markedly accelerating the development of AMD lesions. This is similar to our findings. Our results showed that *Cfh*<sup>+/-</sup> mice exposed to cigarette smoke (causing oxidative stress mainly) exhibited early AMD-like changes, such as RPE cell dysfunction, accumulation of complement activation products, and activation of microglia at 20 weeks (after the 12-week intervention), and that the time to lesion occurrence was significantly shorter. Our findings suggest that the combination of CFH deficiency and smoke exposure promotes rapid AMD-like retinopathy.

As previously mentioned, the pathological changes of the retina caused by smoking are dependent on the activation of the complement system, especially the alternative complement pathway.<sup>17,40</sup> Furthermore, inhibiting the activation of the alternative complement pathway can not only

prevent but also alleviate retinal damage caused by smoking.<sup>18</sup> Collectively, these data suggest a close association among cigarette smoke exposure, hyperactivation of the complement system, and retinopathy.

The disruption of RPE structure and function is one of the pathologic changes of AMD. In our study, RPE cells of *Cfh*<sup>+/-</sup> smoking mice contained more metabolic waste (such as undigested shed photoreceptor outer segments and lipofuscin), and their tight junctions were more severely damaged than RPE cells of WT smoking mice. Both over-activation of the complement system and smoking can lead to an overload of RPE cells, resulting in dysfunction.<sup>41</sup> The RPE dysfunction may affect the photoreceptor metabolism and function, as demonstrated by markedly lower A- and B-wave amplitudes in the *Cfh*<sup>+/-</sup> smoking group than in other groups, including WT smoking mice. We hypothesize that the additional strain of CFH insufficiency weakens the ability of the complement system to protect RPE cells<sup>42</sup> while also hyperactivating the complement system to damage RPE cells.<sup>43</sup> Thus, CFH insufficiency renders RPE cells more susceptible to smoke-induced damage.

Increased autophagy in RPE cells and CFH deficiency have been associated with the formation of depositions, and may contribute to the formation of drusen.<sup>44,45</sup> In our study, *Cfh*<sup>+/-</sup> smoking mice showed accumulation of complement activation products C3b/iC3b/C3c, and OCT revealed drusen-like deposition in the same location. This may be caused by the deficiency of CFH and/or the dysfunction of RPE cells.

### Microglial activation and complement activation

The immune cells of the retina are composed entirely or almost entirely of microglial cells<sup>46</sup>, which play an important role in regulating the inflammatory response. Resting retinal microglia are located in the ganglion cell layer, the inner plexus layer, and the outer plexus layer, while the outer nuclear layer is devoid of microglia. In pathological conditions such as AMD, diabetic retinopathy, and glaucoma, microglia are found in the outer nuclear layer and sub-retinal region.<sup>47,48</sup> We also observed activated microglia cells in *Cfh*<sup>+/-</sup> smoking and WT smoking mice. Microglia activation involves changes in morphology and distribution:<sup>49</sup> microglia transform from a ramified morphology to a hypertrophied or elongated fusiform morphology and migrate to the lesion. Our results showed that the retinal microglial cells in the WT smoking mice were slightly activated, with only dendrites extending into the outer nuclear layer. In the *Cfh*<sup>+/-</sup> smoking mice, microglia were very active, with dendrites reaching the sub-RPE and a large number of microglia migrating to the photoreceptor outer segment layer. Our model shows a phenotype consistent with that of other animal models of early AMD,<sup>10</sup> and it supports the idea that microglial activation contributes to the early pathogenesis of several retinal disorders, including AMD.<sup>47,50</sup>

Abnormal activation of the complement system can directly damage retinal tissue and recruit immune cells into the vicinity of the complement cascade reaction, leading to the infiltration of microglia and chronic



inflammation. Inhibition of complement activation pathways in mice dampens the inflammatory response.<sup>51</sup> Activation of the complement system has a certain influence on the activation of microglial cells.<sup>52</sup> In our study, while no significant differences in C3b/iC3b/C3c deposition (a marker for complement activation) were found between WT and *Cfh*<sup>+/-</sup> smoking mice, microglia activation was higher in the *Cfh*<sup>+/-</sup> smoking mice than in WT smoking mice. Further study should examine the initiators and pathways of microglial activation in our *Cfh*<sup>+/-</sup> smoking animals. Specifically, experiments should explore whether there are differences between *Cfh*<sup>+/-</sup> and WT smoking mice in the whole complement reaction and the reason of different activation of microglia cell between WT and *Cfh*<sup>+/-</sup> smoking mice.

In this study, an early AMD murine model was successfully established by combining smoking exposure and complement over-activation for the first time. The new method greatly shortens the time to achieve the relevant disease phenotype. Future work should observe the animals over longer periods and experiment with different ages at initial exposure, and it may be possible to induce a phenotype that mimics late AMD. And further experiments are needed to elucidate the specific mechanisms underlying the pathological changes of this model.

#### AUTHORS' CONTRIBUTIONS

All authors participated in the design, interpretation of the studies and analysis of the data and review of the article; LF and KN conducted the experiments, LF wrote and edited the article, and WF edited the article.

#### ACKNOWLEDGMENTS

We would like to thank Professor Tao Wang and Dr. Jun Chen from the Respiratory Laboratory of Sichuan University for providing smoking equipment and guidance for animal models. We appreciate the assistance of Professor Song Lei of Sichuan University for technical support with electron microscopy. We thank Professor Danian Chen of Sichuan University for providing us with anti-IB4 antibody.

#### DECLARATION OF CONFLICTING INTERESTS

The author(s) declared no potential conflicts of interest with respect to the research, authorship, and/or publication of this article.

#### FUNDING

The author(s) disclosed receipt of the following financial support for the research, authorship and/or publication of this article: This work was supported by The National Natural Science Foundation of China (81670869 to Wei Fan).

#### ORCID ID

Liwen Feng  <https://orcid.org/0000-0002-2309-8018>

#### SUPPLEMENTAL MATERIAL

Supplemental material for this article is available online.

#### REFERENCES

1. Wu J, Sun X. Complement system and age-related macular degeneration: drugs and challenges. *Drug Des Devel Ther* 2019;**13**:2413–25
2. Mitchell P, Liew G, Gopinath B, Wong TY. Age-related macular degeneration. *Lancet (London, England)* 2018;**392**:1147–59
3. Saunier V, Merle BMJ, Delyfer MN, Cougnard-Gregoire A, Rougier MB, Amouyel P, Lambert JC, Dartigues JF, Korobelnik JF, Delcourt C. Incidence of and risk factors associated with Age-Related macular degeneration: four-year follow-up from the ALIENOR study. *JAMA Ophthalmol* 2018;**136**:473–81
4. Haines JL, Hauser MA, Schmidt S, Scott WK, Olson LM, Gallins P, Spencer KL, Kwan SY, Noureddine M, Gilbert JR, Schetz-Boutaud N, Agarwal A, Postel EA, Pericak-Vance MA. Complement factor H variant increases the risk of age-related macular degeneration. *Science (New York, NY)* 2005;**308**:419–21
5. Edwards AO, Ritter R 3rd, Abel KJ, Manning A, Panhuysen C, Farrer LA. Complement factor H polymorphism and age-related macular degeneration. *Science* 2005;**308**:421–4
6. Ramkumar HL, Zhang J, Chan CC. Retinal ultrastructure of murine models of dry age-related macular degeneration (AMD). *Prog Retin Eye Res* 2010;**29**:169–90
7. Ufret-Vincenty RL, Aredo B, Liu X, McMahon A, Chen PW, Sun H, Niederkorn JY, Kedzierski W. Transgenic mice expressing variants of complement factor H develop AMD-like retinal findings. *Invest Ophthalmol Vis Sci* 2010;**51**:5878–87
8. Coffey PJ, Gias C, McDermott CJ, Lundh P, Pickering MC, Sethi C, Bird A, Fitzke FW, Maass A, Chen LL, Holder GE, Luthert PJ, Salt TE, Moss SE, Greenwood J. Complement factor H deficiency in aged mice causes retinal abnormalities and visual dysfunction. *Proc Natl Acad Sci USA* 2007;**104**:16651–6
9. Toomey CB, Kelly U, Saban DR, Bowes Rickman C. Regulation of age-related macular degeneration-like pathology by complement factor H. *Proc Natl Acad Sci USA* 2015;**112**:E3040–9
10. Landowski M, Kelly U, Klingeborn M, Groelle M, Ding JD, Grigsby D, Bowes Rickman C. Human complement factor H Y402H polymorphism causes an age-related macular degeneration phenotype and lipoprotein dysregulation in mice. *Proc Natl Acad Sci USA* 2019;**116**:3703–11
11. Hoh Kam J, Morgan JE, Jeffery G. Aged complement factor H knockout mice kept in a clean barriered environment have reduced retinal pathology. *Exp Eye Res* 2016;**149**:116–25
12. Smith W, Assink J, Klein R, Mitchell P, Klaver CC, Klein BE, Hofman A, Jensen S, Wang JJ, de Jong PT. Risk factors for age-related macular degeneration: pooled findings from three continents. *Ophthalmology* 2001;**108**:697–704
13. Wang AL, Lukas TJ, Yuan M, Du N, Handa JT, Neufeld AH. Changes in retinal pigment epithelium related to cigarette smoke: possible relevance to smoking as a risk factor for age-related macular degeneration. *PLoS One* 2009;**4**:e5304
14. Cano M, Thimmappula R, Fujihara M, Nagai N, Sporn M, Wang AL, Neufeld AH, Biswal S, Handa JT. Cigarette smoking, oxidative stress, the anti-oxidant response through Nrf2 signaling, and age-related macular degeneration. *Vision Res* 2010;**50**:652–64
15. Fujihara M, Nagai N, Sussan TE, Biswal S, Handa JT. Chronic cigarette smoke causes oxidative damage and apoptosis to retinal pigmented epithelial cells in mice. *PLoS One* 2008;**3**:e3119
16. Wang AL, Neufeld AH. Smoking mice: a potential model for studying accumulation of Drusen-like material on Bruch's membrane. *Vision Res* 2010;**50**:638–42
17. Woodell A, Coughlin B, Kunchithapatham K, Casey S, Williamson T, Ferrell WD, Atkinson C, Jones BW, Rohrer B. Alternative complement pathway deficiency ameliorates chronic smoke-induced functional and morphological ocular injury. *PLoS One* 2013;**8**:e67894

18. Woodell A, Jones BW, Williamson T, Schnabolk G, Tomlinson S, Atkinson C, Rohrer B. A targeted inhibitor of the alternative complement pathway accelerates recovery from smoke-induced ocular injury. *Invest Ophthalmol Vis Sci* 2016;**57**:1728–37
19. Pickering MC, Cook HT, Warren J, Bygrave AE, Moss J, Walport MJ, Botto M. Uncontrolled C3 activation causes membranoproliferative glomerulonephritis in mice deficient in complement factor H. *Nat Genet* 2002;**31**:424–8
20. Cousins SW, Marin-Castano ME, Espinosa-Heidmann DG, Alexandridou A, Striker L, Elliot S. Female gender, estrogen loss, and sub-RPE deposit formation in aged mice. *Invest Ophthalmol Vis Sci* 2003;**44**:1221–9
21. Chen J, Dai L, Wang T, He J, Wang Y, Wen F. The elevated CXCL5 levels in circulation are associated with lung function decline in COPD patients and cigarette smoking-induced mouse model of COPD. *Ann Med* 2019;**51**:314–29
22. Lyzogubov VV, Tytarenko RG, Jha P, Liu J, Bora NS, Bora PS. Role of ocular complement factor H in a murine model of choroidal neovascularization. *Am J Pathol* 2010;**177**:1870–80
23. Moschos MM, Nitoda E. The role of mf-ERG in the diagnosis and treatment of age-related macular degeneration: electrophysiological features of AMD. *Semin Ophthalmol* 2018;**33**:461–9
24. Gerth C. The role of the ERG in the diagnosis and treatment of age-related macular degeneration. *Doc Ophthalmol* 2009;**118**:63–8
25. Owsley C, McGwin G, Jr., Clark ME, Jackson GR, Callahan MA, Kline LB, Witherspoon CD, Curcio CA. Delayed rod-mediated dark adaptation is a functional biomarker for incident early age-related macular degeneration. *Ophthalmology* 2016;**123**:344–51
26. Jackson GR, McGwin G, Jr., Phillips JM, Klein R, Owsley C. Impact of aging and age-related maculopathy on inactivation of the a-wave of the rod-mediated electroretinogram. *Vision Res* 2006;**46**:1422–31
27. van Lookeren Campagne M, Strauss EC, Yaspan BL. Age-related macular degeneration: complement in action. *Immunobiology* 2016;**221**:733–9
28. Xu H, Chen M. Targeting the complement system for the management of retinal inflammatory and degenerative diseases. *Eur J Pharmacol* 2016;**787**:94–104
29. Shaw PX, Zhang L, Zhang M, Du H, Zhao L, Lee C, Grob S, Lim SL, Hughes G, Lee J, Bedell M, Nelson MH, Lu F, Krupa M, Luo J, Ouyang H, Tu Z, Su Z, Zhu J, Wei X, Feng Z, Duan Y, Yang Z, Ferreyra H, Bartsch DU, Kozak I, Zhang L, Lin F, Sun H, Feng H, Zhang K. Complement factor H genotypes impact risk of age-related macular degeneration by interaction with oxidized phospholipids. *Proc Natl Acad Sci USA* 2012;**109**:13757–62
30. Borrás C, Canonica J, Jorieux S, Abache T, El Sanharawi M, Klein C, Delaunay K, Jonet L, Salvodelli M, Naud MC, Arsenijevic Y, Shalabi A, Souchaud L, Behar-Cohen F, Dinét V. CFH exerts anti-oxidant effects on retinal pigment epithelial cells independently from protecting against membrane attack complex. *Sci Rep* 2019;**9**:13873
31. Pons M, Cousins SW, Csaky KG, Striker G, Marin-Castano ME. Cigarette smoke-related hydroquinone induces filamentous actin reorganization and heat shock protein 27 phosphorylation through p38 and extracellular signal-regulated kinase 1/2 in retinal pigment epithelium: implications for age-related macular degeneration. *Am J Pathol* 2010;**177**:1198–213
32. Espinosa-Heidmann DG, Suner IJ, Catanuto P, Hernandez EP, Marin-Castano ME, Cousins SW. Cigarette smoke-related oxidants and the development of Sub-RPE deposits in an experimental animal model of dry AMD. *Invest Ophthalmol Vis Sci* 2006;**47**:729–37
33. Datta S, Cano M, Ebrahimi K, Wang L, Handa JT. The impact of oxidative stress and inflammation on RPE degeneration in non-neovascular AMD. *Prog Retin Eye Res* 2017;**60**:201–18
34. Mettu PS, Wielgus AR, Ong SS, Cousins SW. Retinal pigment epithelium response to oxidant injury in the pathogenesis of early age-related macular degeneration. *Mol Aspects Med* 2012;**33**:376–98
35. Naylor A, Hopkins A, Hudson N, Campbell M. Tight junctions of the outer blood retina barrier. *Ijms* 2019;**21**:211–26
36. Collier RJ, Wang Y, Smith SS, Martin E, Ornberg R, Rhoades K, Romano C. Complement deposition and microglial activation in the outer retina in light-induced retinopathy: inhibition by a 5-HT1A agonist. *Invest Ophthalmol Vis Sci* 2011;**52**:8108–16
37. Woodell A, Rohrer B. A mechanistic review of cigarette smoke and age-related macular degeneration. *Adv Exp Med Biol* 2014;**801**:301–7
38. Ferrington DA, Sinha D, Kaarniranta K. Defects in retinal pigment epithelial cell proteolysis and the pathology associated with age-related macular degeneration. *Prog Retin Eye Res* 2016;**51**:69–89
39. Rowan S, Weikel K, Chang ML, Nagel BA, Thinschmidt JS, Carey A, Grant MB, Fliesler SJ, Smith D, Taylor A. Cfh genotype interacts with dietary glycemic index to modulate age-related macular degeneration-like features in mice. *Invest Ophthalmol Vis Sci* 2014;**55**:492–501
40. Kunchithapautham K, Atkinson C, Rohrer B. Smoke exposure causes endoplasmic reticulum stress and lipid accumulation in retinal pigment epithelium through oxidative stress and complement activation. *J Biol Chem* 2014;**289**:14534–46
41. Georgiannakis A, Burgoyne T, Lueck K, Futter C, Greenwood J, Moss SE. Retinal pigment epithelial cells mitigate the effects of complement attack by endocytosis of C5b-9. *J Immunol* 2015;**195**:3382–9
42. Pauly D, Agarwal D, Dana N, Schäfer N, Biber J, Wunderlich KA, Jabri Y, Straub T, Zhang NR, Gautam AK, Weber BHF, Hauck SM, Kim M, Curcio CA, Stambolian D, Li M, Grosche A. Cell-type-specific complement expression in the healthy and diseased retina. *Cell Rep* 2019;**29**:2835–48 e4
43. Kumar-Singh R. The role of complement membrane attack complex in dry and wet AMD – from hypothesis to clinical trials. *Exp Eye Res* 2019;**184**:266–77
44. Mullins RF, Russell SR, Anderson DH, Hageman GS. Drusen associated with aging and age-related macular degeneration contain proteins common to extracellular deposits associated with atherosclerosis, elastosis, amyloidosis, and dense deposit disease. *FASEB J* 2000;**14**:835–46
45. Wang AL, Lukas TJ, Yuan M, Du N, Tso MO, Neufeld AH. Autophagy, exosomes and Drusen formation in age-related macular degeneration. *Autophagy* 2009;**5**:563–4
46. McMenamin PG, Saban DR, Dando SJ. Immune cells in the retina and choroid: two different tissue environments that require different defenses and surveillance. *Prog Retin Eye Res* 2019;**70**:85–98
47. Rathnasamy G, Foulds WS, Ling EA, Kaur C. Retinal microglia – a key player in healthy and diseased retina. *Prog Neurobiol* 2019;**173**:18–40
48. Zeng XX, Ng YK, Ling EA. Neuronal and microglial response in the retina of streptozotocin-induced diabetic rats. *Vis Neurosci* 2000;**17**:463–71
49. Singaravelu J, Zhao L, Fariss RN, Nork TM, Wong WT. Microglia in the primate macula: specializations in microglial distribution and morphology with retinal position and with aging. *Brain Struct Funct* 2017;**222**:2759–71
50. Penfold PL, Madigan MC, Gillies MC, Provis JM. Immunological and aetiological aspects of macular degeneration. *Prog Retin Eye Res* 2001;**20**:385–414
51. Jiao H, Rutar M, Fernando N, Yednock T, Sankaranarayanan S, Aggior-Bruce R, Provis J, Natoli R. Subretinal macrophages produce classical complement activator C1q leading to the progression of focal retinal degeneration. *Mol Neurodegener* 2018;**13**:45–34
52. Rutar M, Valter K, Natoli R, Provis JM. Synthesis and propagation of complement C3 by microglia/monocytes in the aging retina. *PLoS One* 2014;**9**:e93343

(Received July 15, 2021, Accepted September 17, 2021)